Harvesting the Vibration Energy of $BiFeO_3$ Nanosheets for Hydrogen Evolution

Huilin You[a],[b],[d], Zheng Wu[b],[d],*, Luohong Zhang[b], Yiran Ying[a], Yan Liu[a], Linfeng Fei[a], Xinxin Chen[a], Yanmin Jia[c],[d],*, Yaojin Wang[e], Feifei Wang[f], Sheng Ju[g], Jinli Qiao[h], Chi-Hang Lam[a], and Haitao Huang[a],*

Abstract: Vibration is one of the most prevalent energy sources in natural environment. Here, in this study, mechanical vibration is used for hydrogen generation and decomposition of dye molecules, with the help of $BiFeO_3$ (BFO) square nanosheets. A high hydrogen production rate of ~124.1 μmol/g is achieved under mechanical vibration (100 W) for 1h at the resonant frequency of the BFO nanosheets. The decomposition ratio of Rhodamine B dye is up to ~94.1% after mechanically vibrating the BFO catalyst for 50 min. The vibration induced catalysis of the BFO square nanosheets may be attributed to the piezo-catalytic properties of BFO and the high specific surface area of the nanosheets. The uncompensated piezoelectric charges on the surfaces of BFO nanosheets induced by mechanical vibration result in a built-in electric field across the nanosheets. Unlike a photocatalyst for water splitting, which requires a proper band edge position for hydrogen evolution, such a requirement is not needed in piezo-catalytic water splitting, where the band tilting under the induced piezoelectric field will make the conduction band of BFO more negative than the H_2/H_2O redox potential (0 V) for hydrogen generation. The observed piezo-catalytic properties of BFO nanosheets pave the way towards a non-toxic, highly efficient and sustainable technology for hydrogen generation or dye decomposition through harvesting waste vibration energy from the environment.

Due to the limited fossil-fuels and their serious environmental impact, hydrogen energy has been recognized as an alternative form of clean energy in the future.[1] At present, direct water electrolysis is one of the promising methods for hydrogen production.[2] However, electrolysis has the disadvantage of large consumption of electricity.[2] Since the first report on photocatalytic splitting of water on titanium dioxide (TiO_2) electrodes,[2a] photocatalysis, which can generate electrical charges under light illumination, has demonstrated wide-range applications in the generation of hydrogen fuels and waste water treatment.[1a,1b,2c] TiO_2 quickly becomes one of the most popular materials in solar energy harvesting due to its easy synthesis and low cost.[1a,1b,2a] However, TiO_2 possesses a large bandgap around 3.2 eV and can only absorb ultraviolet light, leading to low efficiency in the utilization of visible solar spectrum.[3]

One approach to increase the solar energy harvesting efficiency is to develop new photocatalytic materials with a bandgap in the visible range.[4] Bismuth ferrite ($BiFeO_3$) is an interesting ferroelectric material for hydrogen generation through photocatalytic water splitting due to its narrow band-gap (~2.2eV) and good chemical stability.[5] The narrow band gap of $BiFeO_3$ allows a large absorption of visible light up to 750 nm, which makes itself an attractive photocatalyst under visible light[6]. For instance, Gao *et al*. used $BiFeO_3$ nanoparticles to decompose methyl orange dye under visible light irradiation.[6] Cho *et al*. applied $BiFeO_3$ nanopowders for the visible light photocatalytic decomposition of Rhodamine B (RhB) dye in water.[7] However, photocatalytic hydrogen generation cannot be achieved by using pure $BiFeO_3$ since its conduction band edge is around 0.33 eV, which is more positive than the H_2/H_2O redox couple potential.[8] The coating of $BiFeO_3$ nanoparticles with a thin layer of $SrTiO_3$ may enable the H_2 evolution under visible light.[8a]

It is noted that $BiFeO_3$ is also ferroelectric and piezoelectric with a large spontaneous polarization in excess of 100 $\mu C \cdot cm^{-2}$ and a piezoelectric coefficient (d_{33}) of ~100 pm/V.[9] It can convert mechanical energy into electric one through the piezoelectric effect.[10] Similar to photocatalysis, where the photo-induced electric charges (electron–hole pairs in photocatalysis) participate in the catalytic redox reactions, in principle, piezoelectric charges (positive and negative ones) induced by mechanical vibrations can also be used to drive catalytic redox reactions, which can be named as piezo-catalysis.[11,12] Although photocatlytic hydrogen evolution is not possible for $BiFeO_3$ due to its more positive conduction band edge than the redox potential for hydrogen evolution reaction (HER), we demonstrate in this work that, large enough piezoelectric field may induce a tilting of the conduction band that makes the HER energetically favorable in $BiFeO_3$ nanoparticles.

Generally, the catalytic performance of a catalyst depends strongly on its surface area and available catalytically active sites.[13] Small size and large surface area of nanoparticles are beneficial to the quick charge transfer between the catalyst and the redox couples to achieve high catalytic activity.[13] Our previous work showed that $NaNbO_3$ nanosheets possess higher pyro-catalytic activity than $NaNbO_3$ nanoparticles.[14] Therefore, in this study, $BiFeO_3$ nanosheets were synthesized to achieve high catalytic activity.

Herein, under mechanical vibration, strong piezo-catalytic hydrogen evolution and dye decomposition are observed with the help of hydrothermally synthesized $BiFeO_3$ nanosheets. Under a mechanical vibration excitation (100 W) for 1h, a hydrogen production rate of about 124.1 μmol/g is achieved. The decomposition ratio of RhB dye can be up to ~94.1% after vibrating $BiFeO_3$ catalyst for 50 min.

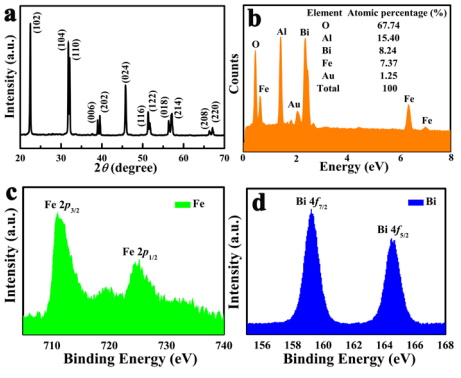

[a] Huilin You, Yiran Ying, Yan Liu, Linfeng Fei, Xinxin Chen, Chi-Hang Lam and Haitao Huang*
Department of Applied Physics and Materials Research Center, The Hong Kong Polytechnic University, Hong Kong SAR, China;
[b] Huilin You, Luohong Zhang and Zheng Wu*
College of Environmental and Chemical Engineering, Xi'an Polytechnic University, Xi'an 710048, China;
[c] Yanmin Jia*
School of Science, Xi'an University of Posts and Communications, Xi'an 710121, China;
[d] Huilin You, Zheng Wu* and Yanmin Jia*
College of Geography and Environmental Science and Department of Physics, Zhejiang Normal University, Jinhua, 321004, China;
[e] Yaojin Wang
School of Materials Science and Engineering, Nanjing University of Science and Technology, Nanjing 210094, China;
[f] Feifei Wang
Department of Physics, Shanghai Normal University, Shanghai, 200235, China;
[g] Sheng Ju
College of Physics, Optoelectronics and Energy and Jiangsu Key Laboratory of Thin Films, Soochow University, Suzhou, 215006, China;
[h] Jinli Qiao
College of Environmental Science and Engineering, State Key Laboratory for Modification of Chemical Fibers and Polymer Materials, Donghua University, Shanghai, 201620, China.
*E-Mail: wuzheng@zjnu.edu.cn (Z. Wu), ymjia@zjnu.edu.cn (Y. Jia) and aphhuang@polyu.edu.hk (H. Huang).

Supporting information for this article is given via a link at the end of the document.

Figure 1 Structural characterizations of the $BiFeO_3$. (a) XRD patterns. (b) EDS spectrum. (c) Fe 2*p* core level XPS spectrum. (d) Bi 4*f* core level XPS spectrum.

The XRD patterns are shown in Figure 1a. All the diffraction peaks can be assigned to a pure rhombohedral phase of $BiFeO_3$ with a space group of *R*3*c* and a point group 3*m* (JCPDS Card no. 86-1518). In Figure 1b, the energy dispersive X-ray spectroscopy (EDS) shows the existence of Bi (8.27%), Fe (7.37%), O (67.74%), Al (15.40%) and Au (1.25%), where Al and Au come from the sample holder and the sputtered Au coating on the powder sample, respectively. XPS was used to investigate the oxidation states of the Bi and Fe elements in $BiFeO_3$. Figure 1c is the high resolution XPS spectrum of Fe 2*p*, showing the binding energy of 711.02 eV for Fe $2p_{3/2}$ and 725.27 eV for Fe $2p_{1/2}$ with a spin orbit splitting of 14.25 eV, which were characteristic for Fe^{3+}.[15] The high resolution XPS spectrum of Bi 4f (Figure 1d) shows two peaks around 159.22 and 164.47 eV, corresponding to Bi $4f_{7/2}$ and Bi $4f_{5/2}$ of the Bi^{3+} state, respectively.[16] Figure S1a is a schematic diagram displaying the circuit for the *P*-*E* hysteresis loop measurement. A well-developed *P*-*E* loop can be observed in Figure S1b, indicating the ferroelectric nature of $BiFeO_3$. The saturation polarization is achieved at an applied electric field of 5.0 $kV \cdot mm^{-1}$.

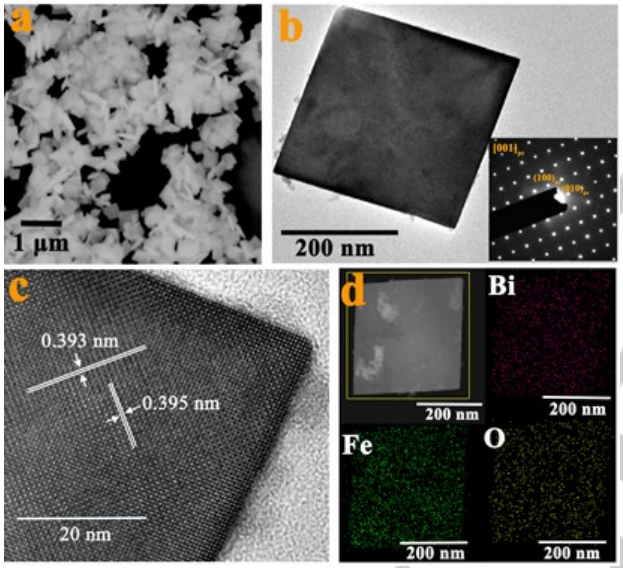

Figure 2 Morphology characterizations of the $BiFeO_3$ nanosheets. (a) SEM image. (b) TEM bright-field image with electron diffraction pattern as inset. (c) High resolution TEM image. (d) Scanning TEM image together with the corresponding elemental mapping.

The SEM and TEM micrographs are shown in Figure 2a and 2b, respectively. The as-prepared $BiFeO_3$ catalyst possesses a morphology of square nanosheet with an average size of ~380 nm. Size distribution of the $BiFeO_3$ nanosheets is shown in Figure S2. The selected area electron diffraction pattern (SAED) is shown in the inset of Figure 2b, indicating the normal direction of $BiFeO_3$ nanosheet being along $[001]_{pc}$ (The subscript "pc" refers to a "pseudo-cubic" structure adopted here for easy indexing). The high resolution TEM image (Figure 2c) of the nanosheet shows two characteristic lattice spacings, both around 0.395 nm, which agree well the *d*-spacings of the $(100)_{pc}$ and $(010)_{pc}$ planes of $BiFeO_3$. Furthermore, the scanning TEM image and the associated elemental mappings of Bi, Fe and O (Figure 2d) show uniform distributions of these elements.

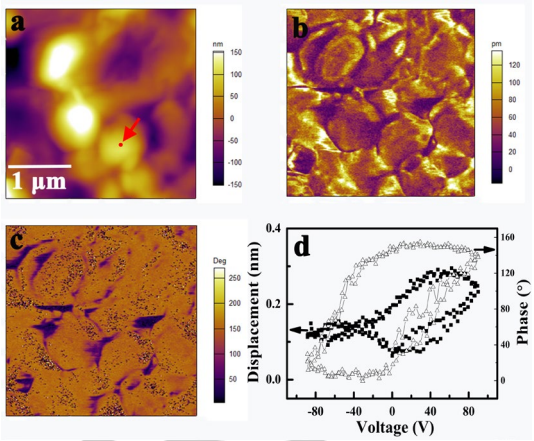

Figure 3 PFM of $BiFeO_3$ nanosheets. (a) Morphology image. (b) Amplitude image. (c) Phase image. (d) Hysteresis loop.

The piezoelectric property of $BiFeO_3$ nanosheets was characterized by a piezoresponse force microscope (PFM), using dual alternating current resonance tracking (DART) modes in order to expel the displacement contribution from electrostatic interaction and topographical crosstalk in mapping the local electromechanical properties. The topographic, vertical piezoresponse amplitude, and phase images of the $BiFeO_3$ nanosheets are shown in Figure 3a-3c, respectively. The $BiFeO_3$ nanosheets can be clearly detected in the topographic image with clear contrasts in the amplitude and phase images. A localized hysteresis loop is observed (Figure 3d), where the phase angle changes by 160° under the reversal of 90 V direct current (DC) bias field, confirming the piezoelectricity of the $BiFeO_3$ nanosheets.

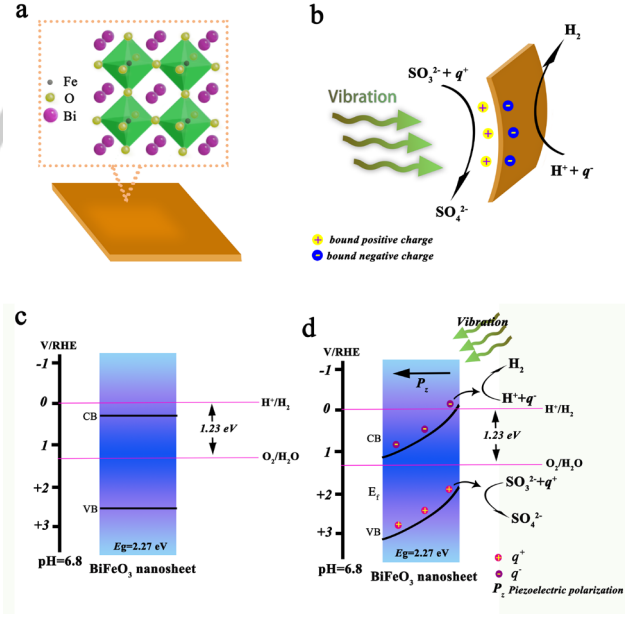

Figure 4 Schematic illustration of the piezo-catalysis mechanism and tilting of energy bands. (a) Atomic structure of $BiFeO_3$. (b) The generation of piezoelectric surface charges under mechanical vibration and the participation of piezo-catalytic hydrogen evolution reaction. (c) Energy band diagram without mechanical vibration. (d) Tilting of energy bands under the strong piezoelectric field induced by mechanical vibration and the accompanied redox reactions.

The basic principle of piezo-catalysis is shown in Figure 4a-b. $BiFeO_3$ nanosheet with a rhombohedral phase is piezoelectric due to the non-central symmetry of its 3*m* point group. When subjected to

mechanical vibration, the thin $BiFeO_3$ nanosheet will easily bend. Due to the piezoelectric effect, lots of positive and negative charges will be generated on the catalyst's surface. The negative electric charges (q^-) generated on the $BiFeO_3$ nanosheets' surfaces will effectively attract the dissociated hydrogen ions in the water to produce H_2. Meanwhile, the positive charges (q^+) accumulated on the other side of the $BiFeO_3$ nanosheets will be consumed by the sacrificial agents (SO_3^{2-}).[17] It should be mentioned that the bandgap of our synthesized $BiFeO_3$ is about 2.27 eV and the flat band potential is 0.32 V *vs*. RHE, as shown in Figure S3. As shown in Figure 4c, the holes generated on the top of valence band (VB) are often energetically favorable for the oxidation of various organic pollutants.[6,7] However, the electrons generated on the bottom of conduction band (CB) is not energetically favorable for hydrogen evolution reaction (HER). Photo-catalytic hydrogen production experiment was conducted to verify that photocatalytic hydrogen generation cannot be achieved by using the synthesized $BiFeO_3$ nanosheets (Figure S4). We show here that the piezoelectric induced internal electric field can tilt the CB and enable the catalytic HER. Under the mechanical deformation of piezoelectric $BiFeO_3$ nanosheets, the open-circuit voltage (V_p) created across the two surfaces of a nanosheet can be calculated as: [12]

$$V_p = \frac{w_3 \cdot T_3 \cdot d_{33}}{\varepsilon_0 \cdot \varepsilon_r} \quad (1)$$

where T_3 is the applied stress in the normal direction of the nanosheet, d_{33} is the piezoelectric moduli, ε_0 is the vacuum permittivity, ε_r is the relative permittivity in the normal direction and w_3 is the thickness of the piezoelectric nanosheet. The applied stress T_3, d_{33}, ε_r of the $BiFeO_3$ nanosheets in the current study are estimated to be about 1.01×10^5 kPa, 100 pm/V, and 26, respectively. [9a,9b,18,19] The thickness of the piezoelectric nanosheet is characterized to be 20 nm according to Atomic force microscopy (AFM) image in Figure S5. The calculated open-circuit voltage across the $BiFeO_3$ nanosheet is about 0.88 V. Based on a rough estimation, the tilting of CB results in the band edge to be lifted up at the negatively charged side, slightly more negative than the H_2/H_2O redox potential (0 V) for HER. Thus, the piezo-catalytic hydrogen generation of water can be realized on pure $BiFeO_3$ material. Equation (1) further implies that the piezo-catalysis can be easily tuned by variation of nanoparticle geometry and materials properties.

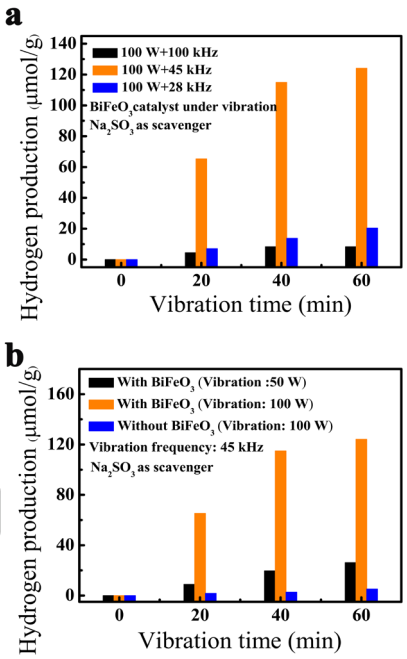

Figure 5 The piezo-catalytic hydrogen production from water splitting under vibration by $BiFeO_3$ nanosheets (a) at different vibration frequencies; (b) with different mechanical power.

Figure 5a shows the piezo-catalytic hydrogen generation result, where the total hydrogen production per gram of catalyst under the vibration power of 100 W for 1 hour is up to 20.4, 124.1, and 8.3 μmol at the frequency of 28, 45, and 100 kHz, respectively. The 1st-order resonance frequency (f^r) of $BiFeO_3$ square nanosheet can be estimated by the following equation,[20]

$$f^r = \frac{\pi}{2}\left[\frac{1}{L^2}+\frac{1}{W^2}\right]\sqrt{\frac{D}{\rho}} \quad (2)$$

where L, W, ρ, and D are the length, width, density, and bending rigidity of the nanosheet, respectively. The bending rigidity D is defined as,

$$D = \frac{E \cdot h^3}{12(1-v^2)} \quad (3)$$

where E, v and h are the Young's modulus, Poisson ratio, and thickness of the material, respectively. For $BiFeO_3$ nanosheet used in this study, these values are about 51 GPa, 0.33, and 20 nm, respectively.[21] Taking the density as 8344 kg/m^3, the resonance frequency of $BiFeO_3$ nanosheet is estimated to be around 46.5 kHz. This result confirms that the highest piezo-catalytic hydrogen generation can be obtained at the resonance frequency of a piezoelectric material (Figure 5a), where the mechanical vibration energy can be more efficiently transferred to the electrical one.

Figure 5b shows the influence of vibration power on hydrogen production. For 1 h mechanical vibration at a frequency of 45 kHz, the hydrogen production of $BiFeO_3$ nanosheet is about 26.1 μmol·g^{-1} under the vibration power of 50 W, which is much lower than that under the vibration power of 100 W. The relationship between the piezoelectric charges (Q) per unit area on the $BiFeO_3$ nanosheet surface, the piezoelectric coefficient (d), and the external stress (T) can be described as $Q=d\cdot T$. Higher vibration power can lead to higher stress T, which induces more piezoelectric charges on the catalyst's surface, resulting in higher hydrogen production rate. Without the catalyst, almost no hydrogen can be generated under the vibration power of 100 W (Figure 5b). It should be noted that although the charge carriers in $BiFeO_3$ are localized and tightly bound,[22] the piezo-generated electrons and holes will be recombined due to conduction across the small nanosheet thickness or vanished due to the quick relaxation of mechanical stress. To suppress the rapid recombination or vanish of the piezoelectrically induced positive and negative charges and increase the lifetime of the negative charges for hydrogen generation, Na_2SO_3 sacrificial agent was used to effectively scavenge the positive charges, similar to what is usually done in photocatalytic hydrogen generation. [17]

The stability of the $BiFeO_3$ nanosheets after 60 min piezo-catalysis can be reflected from the XRD patterns (Figure S6) taken before and after the piezo-catalysis, which are quite similar to each other and no secondary phases can be detected. After piezo-catalysis for 60 mins, a number of cracked nanosheets (Figure S7) were generated due to the high power (100 W) of the ultrasonic machine used. Working at the resonant frequency is another reason that the $BiFeO_3$ nanosheets are easily cracked. This result agrees well with the experimental result (Figure 5) that the hydrogen production rate decreases with increasing reaction time. Decreasing the ultrasound power and tuning the frequency away from resonance will reduce the number of cracked nanosheets. To minimize the effect of temperature on piezo-catalysis, the water in the ultrasonic bath was changed every 20 min. As shown in Figure S8, water temperature change rate was 0.33 °C min^{-1}. The temperature variation was controlled to be below 4 °C.

Density functional theory (DFT) calculations were carried out to study the protonation on the (100) surface of the $BiFeO_3$ nanosheets. It

is found that the H adsorption is energetically favorable on the (100) surface of $BiFeO_3$ (Figure S9). Furthermore, to provide direct evidence of the electro-catalytic activity of $BiFeO_3$ towards hydrogen production, we measured the HER performance of $BiFeO_3$ nanosheets (Figure S10). Hydrogen evolution can be clearly observed at a potential above ~400 mV (Figure S10).

The piezo-catalytic effect was also verified for dye decomposition. Figure S11a shows the piezo-catalytic decomposition of Rhodamine B (RhB) dye under mechanical vibration of $BiFeO_3$ nanosheets. The piezo-catalytic decomposition ratio of RhB dye reaches 94.1% after mechanical vibration for 50 min (Figure S11b) and the RhB dye solution becomes almost completely transparent (inset of Figure S11b). No obvious dye decomposition occurs without the addition of $BiFeO_3$ nanosheets (Figure S11b). Low-frequency piezo-catalytic decomposition of RhB dye was also conducted by mechanical stirring of the solution containing $BiFeO_3$ nanosheets (Figure S12a). Under this low-frequency mechanical stirring, the decomposition ratio of RhB is around 76.4% after 10 h (Figure S12b). The low-frequency piezo-catalytic properties enable the harvesting of waste mechanical energy from environment for water treatment in the future.

Apart from the piezo-catalytic properties of $BiFeO_3$ demonstrated in this work, $BiFeO_3$ is also a proven photocatalyst. [17,19,20,21a] Therefore, a higher hydrogen production rate may be achieved via the combination of piezo-catalysis with photocatalysis, where the simultaneous harvesting of sunlight and natural vibration energy can be realized. There are plenty of rooms for the engineering of the synergistic effect of piezo-catalysis and photocatalysis for enhanced catalytic performance of ferroelectric materials in the future.

For practical applications, it is interesting to note that oceans provide a rich variety of noise sources with a wide range of frequencies. [23] The low-frequency band (10 to 500 Hz) is dominated by commercial shipping and seismic exploration. The medium-frequency band (500 Hz to 500 kHz) is primarily due to sea-surface agitation, various sonars and small vessels. The high-frequency band (>25 kHz) is mainly due to thermal noise. According to equation 2 and 3, the resonant frequency of a piezoelectric material can be tuned by geometry and the selection of material. There are many different kinds of piezoelectric materials, such as, quartz, tourmaline, barium titanate ($BaTiO_3$), lead zirconate titanate (PZT) and its solid solution with lead magnesium niobate (PMN), polyvinylidene fluoride (PVDF), sodium/potassium niobate ($NaNbO_3$, $KNbO_3$), and zinc oxide (ZnO), etc., which add the degree of freedom in materials selection for piezo-catalysis. The availability of the wide frequency spectrum of natural vibration sources makes the harvesting of waste mechanical vibration energy for clean energy generation or environmental pollution treatment very promising. Two possible applications of piezo-catalysis we can envisage at this stage are (1) the utilization of ocean wave vibration for hydrogen evolution and water treatment, and (2) the self-cleaning of the surface of modern buildings, both of which can work together with photocatalysis to obtain some synergistic effects.

In summary, a strong piezo-catalytic hydrogen production via hydrothermally synthesized $BiFeO_3$ square nanosheets is realized at a rate of 124.1 μmol/g under a 100 W vibration excitation at the resonant frequency for 1 h. The piezo-catalytic decomposition ratio of RhB dye can be up to ~94.1% after vibrating $BiFeO_3$ nanosheets for 50 min. The piezo-catalytic property of the $BiFeO_3$ square nanosheets is attributed to the tilting of the conduction band under the strong piezoelectric field induced by mechanical vibration, which make the conduction band more negative than the H_2/H_2O redox potential, enabling the hydrogen evolution. Our work demonstrated that the potential of $BiFeO_3$ for piezo-catalytic hydrogen production via harvesting waste vibration energy from the environment.

Acknowledgements

This work was supported by the National Natural Science Foundation of China (51872264), the Public Welfare Technology Application Research Project of Zhejiang Province, China (LGG18E020005), "ShuGuang" project of Shanghai Municipal Education Commission and Shanghai Education Development Foundation (No. 13SG52), and Shanghai Education Development Foundation (No. 13SG52). This work was also supported by the Hong Kong Polytechnic University (RH9T and RH9G) and the Research Grants Council of the Hong Kong Special Administrative Region, China (Project No. PolyU152665/16E).

Conflict of interest

The authors declare no conflict of interest.

Keywords: Hydrogen • Energy conversion• $BiFeO_3$

References

[1] a) J.A. Turner, *Science*, **2004**, *305*, 972–974; b) S. Park, W.J. Chang, C.W. Lee, S. Park, H. Ahn, K.T. Nam, *Nat. Energy*, **2016**, *2*, 16185; c) P. Zhang, Y. Guo, J. Chen, Y. Zhao, J. Chang, H. Junge, M. Beller and Y. Li, *Nat. Catalysis*, **2018**, *1*, 332–338.

[2] a) A. Fujishima, K. Honda, *Nature*, **1972**, *238*, 37–38; b) D. Das, V.T. Nejat, *Int. J. Hydrogen Energy*, **2001**, *26*, 13–28; c) S. Kazuhior, M. Kazuaki, A. Ryu, A. Yoshimoto, A. Hironori, *J. Photochem. Photobiol.* **2002**, *148*, 71–77; d) S.A. Grigoriev, V.I. Porembsky, V.N. Fateev, *Int. J. Hydrogen Energy,* **2006**, 31, 171-175; e) A. Sartbaeva, V.L. Kuznetsov, S.A. Wells, P.P. Edwards, *Energy Environ. Sci.*, **2008**, 1, 79-85; f) C. Acar, I. Dincer, *Int. J. Hydrogen Energy,* **2014**, 39, 1-12.

[3] K. Awazu, M. Fujimaki, C. Rockstuhl, J. Tominaga, H. Murakami, Y. Ohki, N. Yoshida, T. Watanabe, *J. Am. Chem. Soc.* **2008**, *130*, 1676–1680.

[4] G. Zhang, W. Zhang, Da. Minakata, Y. Chen, J. Crittenden, P. Wang, *Int. J. Hydrogen Energy*, **2013**, *38*, 11727–11736.

[5] a) S. R. Basu, L. W. Martin, Y. H. Chu, M. Gajek, R. Ramesh, R. C. Rai, X. Xu, J. L. Musfeldt, *Appl. Phys. Lett.* **2008**, *92*, 091905; b) T. Choi, S. Lee, Y. J. Choi, V. Kiryukhin, S.-W. Cheong, *Science*, **2009,** *324*, 63–66.

[6] F. Gao, X. Chen, K. Yin, S. Dong, Z. Ren, F. Yuan, T. Yu, Z. Zou, J.M. Liu, *Adv. Mater*. **2007**, *19*, 2889–2892.

[7] C. Cho, J. Noh, I.-S. Cho, J.-S. An, K. Hong, *J Am Ceram Soc,* **2008**, *91*, 3753–3755.

[8] a) J. Luo, P. A. Maggard, *Adv Mater*, **2006**, *18*, 514–517; b) L. Di, H. Yang, T. Xian, X. Chen, *Mat. Res.* **2018**, *21*, e20180081.

[9] a) J.M. Park, S. Nakashima, M. Sohgawa, T. Kanashima, M. Okuyama, *Jpn. J. Appl. Phys.* **2012**, *51*, 09MD05; b) S. K. Singh, H. Ishiwara, K. Maruyama, *Appl. Phys. Lett.* **2006**, *88*, 262908.

[10] a) A. Marino, and R. Becker, *Nature*, **1970**, *228*, 473–474; b) I. Katsouras, K. Asadi, M. Li, T.B. van Driel, K.S. Kjær, D. Zhao, T. Lenz, Y. Gu, P.W.M. Blom, D. Damjanovic, M.M. Nielsen, D.M. de Leeuw, *Nat Mater.* **2016**, *15*, 78–84.

[11] Y.M. Jia, H. S. Luo, X.Y. Zhao, F.F.Wang, *Adv. Mat.* **2008**, *20*, 4776–4779.

[12] M.B. Starr, X. Wang, *Sci. Rep.* **2013**, *3*, 2160.

[13] a) Y. Li, Z. Ping, *J. Am. Chem. Soc.* **2011**, *133*, 15743–15752; b) Y. Zhang, M. Xie, V. Adamaki, H. Khanbareh, C.R. Bowen, *Chem. Soc. Rev.* **2017**, *46*, 7757–7786.

[14] H. You, Z. Wu, L. Wang, Y. Jia, S. Li and J. Zou, *Chemosphere*, **2018**, *199*, 531–537.

[15] J. Zhou, R. Yang, R. Xiao, X. Chen, C. Deng, *Mater. Res. Bull.* **2012**, *47*, 3630–3636.
[16] A. Jaiswal, R. Das, K. Vivekanand, P.M. Abraham, S. Adyanthaya, P. Poddar, *J. Phys. Chem. C*, **2010**, *114*, 2108–2115.
[17] L. Lu, M. Lv, G. Liu, X. Xu, *Appl. Surf. Sci.* **2017**, *391*, 535–541.
[18] a) M. Dükkancı, G. Gündüz, *Ultrason. Sonochem.* **2006**, *13*, 517–522; b) M.C. Saha, Md.E. Kabir, S. Jeelani, *Mater. Sci. Eng., A,* **2008**, *479*, 213–222; c) M.A. Behnajady, N. Modirshahla, S. Bavili Tabrizi, S. Molanee, *J. Hazard. Mater.* **2008**, *152*, 381–386.
[19] Y.A. Chaudhari, C.M. Mahajan, E.M. Abuassaj, P.P. Jagtap, P.B. Patil, S.T. Bendre, *Mater. Sci-Poland*, **2013**, *31*, 221–225.
[20] M.C. Junger, D. Feit, **1986**, *Cambridge*, MA: MIT press.
[21] a) P. Sen, A. Dey, A.K. Mukhopadhyay, S.K. Bandyopadhyay, A.K. Himanshu, *Ceram. Int.* 2012, *38*, 1347–1352; b) M.K. Yaakob, M.F.M. Taib, L. Lu, O.H. Hassan, M.Z.A. Yahya, *Mater. Res. Express,* **2015**, *2*, 116101.
[22] H. Huang, *Nat. Photon.* **2010**, *4*, 134–135.
[23] a) J.A. Hildebrand, Mar. Ecol. Prog. Ser. **2009**, 395, 5-20; b) W.M. Carey, M.P. Bradley, *J. Acoust. Soc. Am. Suppl.* **1985**, 78, S2; c) J.A. Scrimger, D.J. Evans, W. Yee, *J. Acoust. Soc. Am.* **1989**, 85, 726–731.

COMMUNICATION

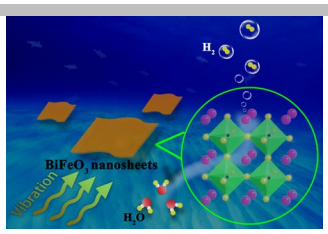

$BiFeO_3$ is piezo-catalytic active in hydrogen production via harvesting vibration energy from environment. The strong piezoelectric field induced by mechanical vibration tilts the conduction band of $BiFeO_3$, making it more negative than the H_2/H_2O redox potential to enable the hydrogen evolution. (see picture)

Huilin You, Zheng Wu, Luohong Zhang, Yiran Ying, Yan Liu, Linfeng Fei, Xinxin Chen, Yanmin Jia*,Yaojin Wang, Feifei Wang, Sheng Ju, Jinli Qiao, Chi-Hang Lam, and Haitao Huang**
Page No. – Page No.

Harvesting the Vibration Energy of $BiFeO_3$ Nanosheets for Hydrogen Evolution